Thalamus parcellation using multi-modal feature classification and thalamic nuclei priors

Jeffrey Glaister[a], Aaron Carass[a,b], Joshua V. Stough[c],
Peter A. Calabresi[d], and Jerry L. Prince[a]

[a]Dept. of Electrical and Computer Engineering,
Johns Hopkins University, Baltimore, MD 21218, USA
[b]Dept. of Computer Science, Johns Hopkins University, Baltimore, MD 21218, USA
[c]Dept. of Computer Science, George Mason University, Fairfax, VA 22030, USA
[d]Dept. of Neurology, Johns Hopkins School of Medicine, Baltimore, MD 21287, USA

ABSTRACT

Segmentation of the thalamus and thalamic nuclei is useful to quantify volumetric changes from neurodegenerative diseases. Most thalamus segmentation algorithms only use T1-weighted magnetic resonance images and current thalamic parcellation methods require manual interaction. Smaller nuclei, such as the lateral and medial geniculates, are challenging to locate due to their small size. We propose an automated segmentation algorithm using a set of features derived from diffusion tensor image (DTI) and thalamic nuclei location priors. After extracting features, a hierarchical random forest classifier is trained to locate the thalamus. A second random forest classifies thalamus voxels as belonging to one of six thalamic nuclei classes. The proposed algorithm was tested using a leave-one-out cross validation scheme and compared with state-of-the-art algorithms. The proposed algorithm has a higher Dice score compared to other methods for the whole thalamus and several nuclei.

Keywords: Diffusion MRI, magnetic resonance imaging, machine learning, segmentation, thalamus parcellation

1. INTRODUCTION

The thalamus is an important subcortical structure that plays a crucial role in relaying sensory and motor signals to the cerebral cortex and regulating consciousness, sleep, and alertness.[1] It has connections to nearly every major region in the brain. Changes in thalamic volume are correlated with many neurodegenerative diseases, including multiple sclerosis,[2] Alzheimer's disease,[3,4] and schizophrenia.[5] The thalamus is composed of myelinated fibers and can be divided into thalamic nuclei. The thalamic nuclei include the anterior (ANT), medial dorsal (MD), ventral nuclear group (VNG), pulvinar (PUL), lateral geniculate (LGN), and medial geniculate (MGN). Nuclei are clusters of neurons grouped based on histological or functional criteria.[6] Diffusion tensor imaging (DTI) is a magnetic resonance (MR) imaging modality that images the diffusion rate of water and can be used to infer the orientation of neural fibers.[7] With the strong connections that the thalamus has with other structures, DTI offers a rich set of features to use to segment the thalamus and its nuclei.

Several existing whole thalamus segmentation methods use T1-weighted (T1-w) MRI[8,9] and do not take advantage of DTI features. Existing thalamic nuclei methods require manual interaction in order to initialize the segmentation algorithm.[10–13] In our previous work,[14,15] a comprehensive set of features derived from DTI were used to segment the thalamic nuclei. However, segmenting the LGN and MGN is still challenging due to their small size and remote locations relative to the rest of the thalamus. Structure location priors derived from a manual delineated atlas have been used to segment subcortical structures by registering the brain template to the subject image. We propose deriving thalamic nuclei location priors for each nucleus using a manually delineated brain atlas to augment the classification features and better resolve the lateral and medial geniculates.

Further author information: (Send correspondence to J. Glaister)
J. Glaister: E-mail: jglaist1@jhu.edu

We present a fully automatic multi-modal thalamus segmentation algorithm that incorporates DTI features and nuclei location priors. Our method first identifies a region of interest (ROI) containing the thalamus from location priors derived from a delineated brain template. For each voxel in the ROI, a set of features is derived from the DTI, T1-w, T2-weighted (T2-w) MRI, and priors. A hierarchical random forest (RF) classifier framework is trained to first distinguish between thalamus and non-thalamus voxels in the ROI. A second RF classifies the thalamus voxels as one of six thalamic nuclei.

2. METHOD

The initial subject images first undergo standard neuroimaging preprocessing: inhomogeneity correction,[16] skull stripping,[17] isotropic resampling[18] to 0.8 mm cubic voxels, and distortion correction.[19]

2.1 Thalamus Localization and Thalamic Nuclei Priors

An initial estimate of the location of the thalamus is determined by registering a brain atlas to the subject's T1-w using the Elastix deformable registration algorithm[20] and deforming the atlas labels to be aligned with the subject's image to give us an initial segmentation for each nucleus, $\mathcal{N}_i$ for $i \in \{\text{ANT}, \text{MD}, \text{VNG}, \text{PUL}, \text{LGN}, \text{MGN}\}$. The union of these is the initial thalamus segmentation, $\mathcal{T}$. The ICBM Brain Template[21] is used as the brain atlas.

These initial segmentations are used to calculate both the ROI and nuclei priors. All initial segmentations are divided into left and right segmentations along the midsagittal plane[22] giving $\mathcal{T}_L$ and $\mathcal{T}_R$. However, to simplify notation and because the algorithm is applied to left and right sides independently, we will drop the subscript and continue to use $\mathcal{T}$ to refer to the initial segmentation of the thalamus on either side. The ROI for the thalamus is found by constructing a bounding box, $\mathcal{B}$ that encompasses all voxels labeled as thalamus. $\mathcal{B}$ is defined as

$$\mathcal{B} = \{\boldsymbol{x} | (\boldsymbol{l} - \boldsymbol{r}) \leq \boldsymbol{x} \leq (\boldsymbol{h} + \boldsymbol{r}), \boldsymbol{x} \in \Omega\},$$

where vector $\boldsymbol{x}$ is a voxel coordinate in the image domain Ω, the lower and upper extents of the thalamus are given by $\boldsymbol{l} = \arg\min_{\boldsymbol{x} \in \mathcal{T}} \boldsymbol{x}$ and $\boldsymbol{h} = \arg\max_{\boldsymbol{x} \in \mathcal{T}} \boldsymbol{x}$ respectively, and $\boldsymbol{r} = 0.2 \times (\boldsymbol{h} - \boldsymbol{l})$ pads the bounding box by 20% along each axis.

The set of nuclei location priors $\{P_i\}$ is constructed from the initial thalamic nuclei segmentations $\{\mathcal{N}_i\}$ by convolving $\mathcal{N}_i$ with a 3-D Gaussian kernel with standard deviation σ. Similarly, the thalamus location prior P_T is constructed by convolving $\mathcal{T}$ with the Gaussian kernel.

2.2 Feature Extraction

Various features are extracted from the T1-w, T2-w, and DTI. The first features are the voxel location, $\boldsymbol{x}$, and the T1-w intensity and T2-w intensity, denoted as $I_{\text{T1}}(\boldsymbol{x})$ and $I_{\text{T2}}(\boldsymbol{x})$.

A set of features is derived from the DTI. DTI is acquired from a set of diffusion weighted MRI with known b-value and gradient direction $\boldsymbol{g}$. The diffusion signal at a particular b and $\boldsymbol{g}$ is an attenuated version of the signal S_0 recording in absence of the any diffusion weighting, whose relationship can be expressed using the Stejskal-Tanner equation

$$S(b, \boldsymbol{g}) = S_0 e^{-b\boldsymbol{g}^T D \boldsymbol{g}}.$$

The diffusion tensor D is represented by a 3×3 symmetric tensor matrix that quantifies the diffusivity at a voxel. Alternatively, the tensor can be expressed in terms of its eigenvalues and eigenvectors. Two features derived from the eigenvalues of D are the fractional anisotropy $\text{FA}(\boldsymbol{x})$ and mean diffusivity $\text{MD}(\boldsymbol{x})$.[7]

The direction of maximum diffusion corresponds to the principal eigenvector (PEV), $\boldsymbol{u} = (u_1, u_2, u_3)$. Since diffusion can occur with equal probability along $\boldsymbol{u}$ and the opposite direction $-\boldsymbol{u}$, it is convenient to use the Knutsson space instead to represent the PEV.[23] The Knutsson transformation maps $\boldsymbol{u}$ and $-\boldsymbol{u}$ to the same 5-D vector $\{K(\boldsymbol{x})\}$ in Knutsson space. The transformation from $\mathbb{R}^3$ to Knutsson space $\mathbb{K} \subset \mathbb{R}^5$ is

$$\boldsymbol{K}(u_1, u_2, u_3) = (u_1^2 - u_2^2, 2u_1u_2, 2u_1u_3, 2u_2u_3, \frac{1}{\sqrt{3}}(2u_3^2 - u_1^2 - u_2^2)).$$

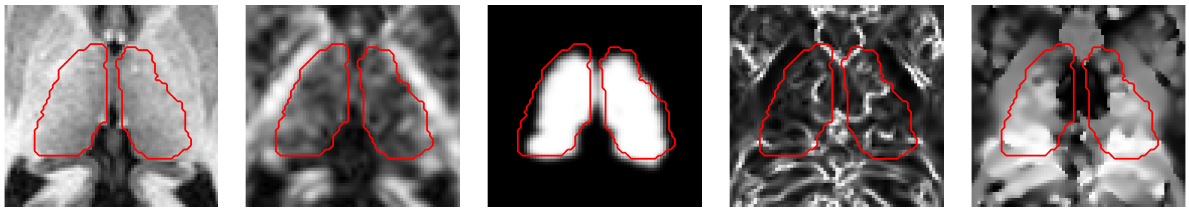

(a) T1-w (b) FA (c) Thalamus Prior (d) Edge Map (e) 1st Knutsson Dir.

Figure 1: Shown are several of the features used in our approach. The red outline indicates the manually delineated ground truth.

To distinguish between thalamic nuclei, we are interested in finding locations with large changes in the direction of the PEV. Letting $\boldsymbol{v}$ be the PEV transformed to the Knutsson space, then the amount of change in the PEV direction can be quantified as the Frobenius norm $||G(K(\boldsymbol{x}))||_F$ of the edge map of the Knutsson space,[24] as follows:

$$G(\boldsymbol{v}) = \begin{bmatrix} \frac{\partial v_1}{\partial x} & \frac{\partial v_1}{\partial y} & \frac{\partial v_1}{\partial z} \\ \vdots & \vdots & \vdots \\ \frac{\partial v_5}{\partial x} & \frac{\partial v_5}{\partial y} & \frac{\partial v_5}{\partial z} \end{bmatrix} \qquad ||G(\boldsymbol{v})||_F = \sqrt{\sum_i \sum_j G(\boldsymbol{v})_{ij}^2}.$$

The final set of features is the location and thalamus prior, resulting in a feature vector $\boldsymbol{f}_T$ with the following 14 features: $\boldsymbol{f}_T(\boldsymbol{x}) = \{\boldsymbol{x}, I_{\text{T1}}(\boldsymbol{x}), I_{\text{T2}}(\boldsymbol{x}), \text{FA}(\boldsymbol{x}), \text{MD}(\boldsymbol{x}), \{K(\boldsymbol{x})\}, ||G(K(\boldsymbol{x}))||_F, P_T(\boldsymbol{x})\}$. Similarly, to classify the thalamus voxels as belonging to one of the six thalamic nuclei, we include the six nuclei priors in the feature vector $\boldsymbol{f}_N$, resulting in 19 features: $\boldsymbol{f}_N(\boldsymbol{x}) = \{\boldsymbol{x}, I_{\text{T1}}(\boldsymbol{x}), I_{\text{T2}}(\boldsymbol{x}), \text{FA}(\boldsymbol{x}), \text{MD}(\boldsymbol{x}), \{K(\boldsymbol{x})\}, ||G(K(\boldsymbol{x}))||_F, \{P_i(\boldsymbol{x})\}\}$. Figure 1 shows the features extracted for segmenting the thalamus with the ground truth outlined in red.

2.3 Hierarchical Random Forest Classification

Our hierarchical RF approach consists of two steps. First, the feature vectors $\boldsymbol{f}_T$ for each voxel in B are used to build a collection of trees that distinguish thalamus from non-thalamus. The result of this RF is a binary classification. The largest connected component in the binary map is smoothed using a morphological closing operation with a $3 \times 3 \times 3$ structuring element. This gives the final thalamus segmentation. The second RF is trained using $\boldsymbol{f}_N$ as the feature vectors to classify voxels inside the final thalamus segmentation as belonging to one of the six thalamic nuclei classes. Separate RFs are trained for the left and right sides.

3. RESULTS AND DISCUSSION

Our data consists of five subjects from an multiple sclerosis (MS) study with manually delineated ground truth. Three of the subjects are diagnosed with MS and the remaining two are healthy controls (HC). A leave-one-out cross validation scheme is used to train and test the proposed algorithm. The thalamus segmentation results are compared with two state-of-the-art algorithms; TOADS[8] and FreeSurfer.[9] Both are atlas-based subcortical segmentation algorithms and provide a whole thalamus label. Results are also compared with the initial thalamus segmentation determined by transferring labels from the ICBM brain template[21] (referred to as Label Transfer), as is done to acquire the priors.

Examples of whole thalamus segmentation using the proposed algorithm and other state-of-the-art algorithms are shown in Figure 2. The mean Dice scores are provided in Table 1 with the proposed algorithm outperforming the other algorithms. The label transfer algorithm has the second best Dice scores. However, the label for the lateral geniculate in the brain atlas is not contiguous with the rest of the thalamus, resulting in the thalamus being split into separate parts. The proposed algorithm uses a set of manual delineations with the lateral geniculate joined with the rest of the thalamus to train the random forest and as a result, the lateral geniculate is connected to the thalamus. A connected-component analysis ensures that only a single connected component is returned as the final thalamus segmentation.

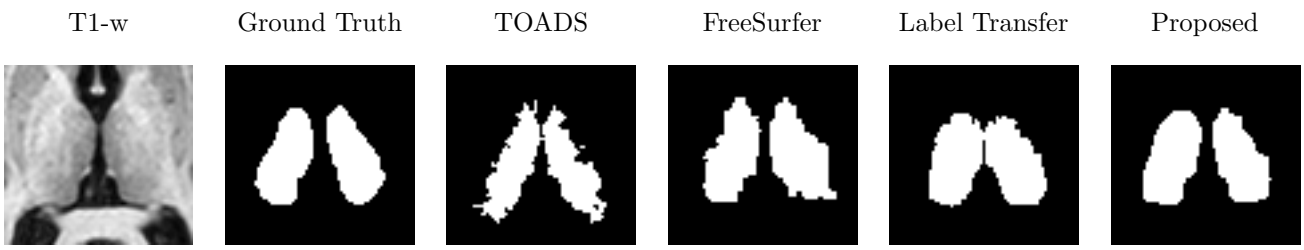

(a) Subject 1 (MS)

(b) Subject 2 (HC)

(c) Subject 3 (HC)

Figure 2: From left to right are: T1-w; manually delineated ground truth; TOADS; FreeSurfer; Label Transfer from the ICBM atlas; and our proposed algorithm.

Table 1: Mean (standard deviation) of Dice scores comparing whole thalamus segmentation.

Structure	**TOADS**	**FreeSurfer**	**Label Transfer**	**Proposed**
Left Thalamus	0.522 (0.120)	0.811 (0.025)	0.766 (0.055)	0.881 (0.024)
Right Thalamus	0.566 (0.130)	0.783 (0.074)	0.779 (0.055)	0.859 (0.040)

An example of the thalamic nuclei segmentation using the proposed algorithm and the label transfer algorithm is shown in Figure 3. The Dice scores of the proposed algorithm and the ICBM algorithm for each of the nuclei are provided in Table 2. The proposed algorithm outperforms the label transfer algorithm for eleven of the twelve thalamic nuclei. Only the left medial geniculate Dice score is lower using the proposed algorithm. This is due to the location of the medial geniculate, as the proposed algorithm often misclassifies MGN as the pulvinar. Other errors in the proposed algorithm's nuclei parcellation are caused by the hierarchical random forest scheme. The nuclei segmentation relies directly on the segmentation of the thalamus. This is especially relevant to the LGN and MGN, which has the lowest nuclei Dice scores because many of the voxels are classified as non-thalamus and are excluded from the nuclei classification step.

4. CONCLUSION

We have presented a fully automatic thalamic parcellation algorithm using multi-modal imaging data and nuclei priors. The algorithm extracts a set of features derived from T1-w, T2-w, and DTI to train a hierarchical RF framework. For whole thalamus segmentation, the proposed algorithm has higher Dice scores of 0.881 and 0.859 for the left and right thalamus, respectively. The proposed algorithm also improved Dice scores for individual thalamic nuclei, in particular the smaller nuclei, such as the lateral and medial geniculates.

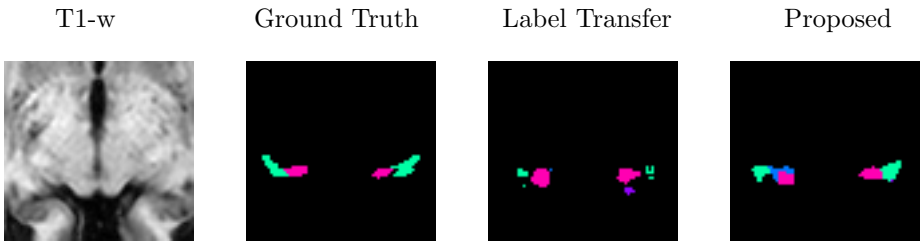

(a) Subject 1 (MS) Geniculates

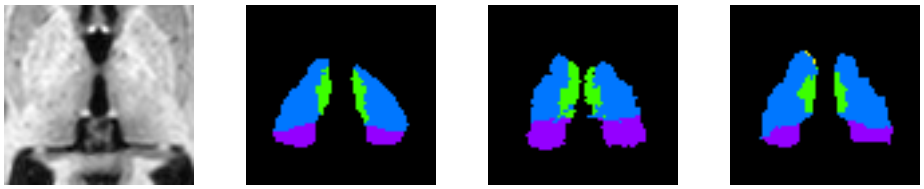

(b) Subject 1 (MS) Nuclei

Figure 3: Example thalamic nuclei segmentation from left to right are: T1-w; manually delineated ground truth; Label Transfer from the ICBM atlas; and our proposed algorithm. Nuclei shown are: VNG (blue); MD (green); PUL (purple); LGN (turquoise); and MGN (pink).

Table 2: Mean Dice scores comparing the thalamic nuclei segmentation.

Algorithm	**Left**					
	ANT	**MD**	**LGN**	**VNG**	**PUL**	**MGN**
Label Transfer	0.159	0.562	0.314	0.667	0.580	0.475
Proposed	0.485	0.667	0.431	0.785	0.700	0.375
Algorithm	**Right**					
	ANT	**MD**	**LGN**	**VNG**	**PUL**	**MGN**
Label Transfer	0.133	0.498	0.254	0.670	0.554	0.461
Proposed	0.432	0.581	0.410	0.757	0.655	0.479

ACKNOWLEDGMENTS

This project is funded by the NIH/NINDS through grant 1R21NS082891. Jeffrey Glaister is funded in part by the National Science and Engineering Research Council of Canada.

REFERENCES

[1] Sherman, S. M. and Guillery, R., [*Exploring the Thalamus*], Elsevier (2000).

[2] Cifelli, A. et al., "Thalamic neurodegeneration in multiple sclerosis," *Annals of Neurology* **52**(5), 650–653 (2002).

[3] Braak, H. and Braak, E., "Alzheimer's disease affects limbic nuclei of the thalamus," *Acta Neuropathologica* **81**(3), 261–268 (1991).

[4] Zarei, M. et al., "Combining shape and connectivity analysis: An MRI study of thalamic degeneration in alzheimer's disease," *NeuroImage* **49**(1), 1 – 8 (2010).

[5] Byne, W. et al., "Postmortem assessment of thalamic nuclear volumes in subjects with schizophrenia," *Am. J. Psychiatry* **159**(1), 59–65 (2002).

[6] Ziyan, U., Tuch, D., and Westin, C. F., "Segmentation of Thalamic Nuclei from DTI Using Spectral Clustering," in [*9th International Conference on Medical Image Computing and Computer Assisted Intervention (MICCAI 2006)*], **4191**, 807–814 (2006).

[7] Westin, C.-F. et al., "Processing and visualization for diffusion tensor MRI," *Medical Image Analysis* **6**(2), 93–108 (2002).

[8] Bazin, P. L. and Pham, D. L., "Homeomorphic brain image segmentation with topological and statistical atlases," *Medical Image Analysis* **12**(5), 616–625 (2008).

[9] Fischl, B. et al., "Whole brain segmentation: Automated labeling of neuroanatomical structures in the human brain," *Neuron* **33**, 341–355 (Jan. 2002).

[10] Duan, Y., Li, X., and Xi, Y., "Thalamus segmentation from diffusion tensor magnetic resonance imaging," *International Journal of Biomedical Imaging* **5**(2), 1–5 (2007).

[11] Jonasson, L. et al., "A level set method for segmentation of the thalamus and its nuclei in DT-MRI," *Signal Processing* **87**(2), 309–321 (2007).

[12] Rittner, L. et al., "Segmentation of thalamic nuclei based on tensorial morphological gradient of diffusion tensor fields," in [*7th International Symposium on Biomedical Imaging (ISBI 2010)*], 1173–1176 (2010).

[13] Wiegell, M. R. et al., "Automatic segmentation of thalamic nuclei from diffusion tensor magnetic resonance imaging," *NeuroImage* **19**(2), 391–401 (2003).

[14] Stough, J. V. et al., "Thalamic parcellation from multi-modal data using random forest learning," in [*10th International Symposium on Biomedical Imaging (ISBI 2013)*], 852–855 (2013).

[15] Stough, J. V. et al., "Automatic method for thalamus parcellation using multi-modal feature classification," in [*17th International Conference on Medical Image Computing and Computer Assisted Intervention (MICCAI 2014)*], (2014).

[16] Sled, J. G. et al., "A non-parametric method for automatic correction of intensity non-uniformity in MRI data," *IEEE Trans. Med. Imag.* **17**(1), 87–97 (1998).

[17] Carass, A. et al., "Simple paradigm for extra-cerebral tissue removal: Algorithm and analysis," *NeuroImage* **56**(4), 1982–1992 (2011).

[18] Thévenaz, P., Blu, T., and Unser, M., "Interpolation revisited [medical images application]," *IEEE Trans. Med. Imag.* **19**(7), 739–758 (2000).

[19] Studholme, C. et al., "Accurate alignment of functional EPI data to anatomical MRI using a physics-based distortion model," *IEEE Trans. Med. Imag.* **19**(11), 1115–1127 (2000).

[20] Klein, S. et al., "Elastix: A toolbox for intensity-based medical image registration," *IEEE Trans. Med. Imag.* **29**, 196–205 (Jan 2010).

[21] Mazziotta, J. C. et al., "A probabilistic atlas of the human brain: theory and rationale for its development. The International Consortium for Brain Mapping (ICBM)," *NeuroImage* **2**(2), 89–101 (1995).

[22] Anbazhagan, P. et al., "Automatic estimation of midsagittal plane and AC-PC alignment on nonrigid registration," in [*3rd International Symposium on Biomedical Imaging (ISBI 2006)*], 828–831 (2006).

[23] Knutsson, H., "Producing a continuous and distance preserving 5-D vector representation of 3-D orientation," in [*IEEE Computer Society Workshop on Computer Architecture for Pattern Analysis and Image Database Management*], 175–182 (1985).

[24] Fan, X. et al., "A novel contrast for DTI visualization for thalamus delineation," *Proceedings of SPIE Medical Imaging (SPIE-MI 2010), San Diego, CA, February 14-17, 2010* **7625**, 762533–762533–9 (2010).